

The Role of the Bottom Relief and the β -effect in the Black Sea Dynamics

A. A. Pavlushin*, N. B. Shapiro, E. N. Mikhailova

Marine Hydrophysical Institute, Russian Academy of Sciences, Sevastopol, Russian Federation

*e-mail: pavlushin@mhi-ras.ru

The results of the numerical experiments carried out within the two-layer eddy-resolving Black Sea model are discussed. The motion of the liquid is excited by a stationary wind with a constant cyclonic vorticity. Bottom relief, β -effect, bottom friction and horizontal turbulent viscosity parameterized by the bi-harmonic operator are taken into account in the model. Friction on the interface of the layers is not taken into account, thus, the motion in the lower layer is excited only by non-linear factors. The calculations cover a long period (20 years) up to the moment when the solution achieves the statistically equilibrium mode which is characterized by presence of intense currents, waves and eddies. It is shown that under the statistically equilibrium mode, a cyclonic circulation is formed in the sea: in the upper layer – a meandering flow (the Rim Current analog); in the lower layer – rather intensive waves which are imposed on the flow propagating along the isobaths. These waves can be characterized as the topographic Rossby waves trapped by the continental slope. The technique for analyzing such waves is proposed. It is shown that the current wave disturbances in the lower layer significantly influence the flows in the upper layer contributing to their instability and meandering.

Keywords: the Black Sea, eddy resolving model, numerical experiment, β -effect, topographic Rossby waves, bottom relief, trapped waves.

DOI: 10.22449/1573-160X-2017-6-24-35

© 2017, A. A. Pavlushin*, N. B. Shapiro, E. N. Mikhailova

© 2017, Physical Oceanography

Introduction. Within the framework of a two-layer eddy-resolving model, the results of a study of the bottom relief and the β -effect influence on the circulation formation in the Black Sea under the effect of a stationary cyclonic wind with constant vorticity are presented in the present paper. It is a continuation of a series of numerical experiments [1, 2], devoted to the modeling of wind circulation in the Black Sea. In the previously published papers, the results of numerical experiments on the role of such factors as wind vorticity, basin shape, coastline orography, bottom friction intensity and horizontal turbulent viscosity, the β -effect in cases where the bottom relief was not taken into account (the bottom was assumed to be horizontal) are discussed.

The model is based on primitive equations of ocean hydrodynamics [3]. The equations of the model are vertically integrated within the boundaries of each layer of the equation of motion and continuity

$$(U_1)_t + (u_1 U_1)_x + (v_1 U_1)_y - fV_1 = gh_1 \zeta_x + \tau^x - R_a^x + A_B \nabla (h_1 \nabla (\Delta u_1)),$$

$$(V_1)_t + (u_1 V_1)_x + (v_1 V_1)_y + fU_1 = gh_1 \zeta_y + \tau^y - R_a^y + A_B \nabla (h_1 \nabla (\Delta v_1)),$$

$$(U_2)_t + (u_2 U_2)_x + (v_2 U_2)_y - fV_2 = gh_2 \zeta_x + g'h_2 (h_1)_x + R_a^x - R_b^x + A_B \nabla (h_2 \nabla (\Delta u_2)),$$

$$(V_2)_t + (u_2 V_2)_x + (v_2 V_2)_y + fU_2 = gh_2 \zeta_y + g'h_2 (h_1)_y + R_a^y - R_b^y + A_B \nabla (h_2 \nabla (\Delta v_2)),$$

$$\begin{aligned}(h_1)_t + (U_1)_x + (V_1)_y &= 0, \\ (h_2)_t + (U_2)_x + (V_2)_y &= 0,\end{aligned}$$

where indices 1 and 2 denote the layer number; the lower indices x, y and t designate differentiation; u_k, v_k are the k -layer horizontal components of the current velocity directed along the X (to the east) and Y (to the north) axes, respectively; h_1, h_2 are the layer thickness; $U_k = u_k h_k, V_k = v_k h_k$ are the flow components in the layers; R_a^x, R_a^y are the components of the friction force between the layers; R_b^x, R_b^y are the bottom friction force components; $f = f_0 + \beta y$ is the Coriolis parameter, $f_0 = 10^{-4}$ 1/s, $\beta = 2 \cdot 10^{-13}$ 1/(cm·s); $g = 980$ g·cm/s² is the free fall acceleration; $g' = g(\rho_2 - \rho_1)/\rho_2$; τ^x, τ^y are the tangential wind stress components; A_l is the horizontal eddy viscosity coefficient.

The integral continuity equation in the rigid lid approximation terminates the equations:

$$U_x + V_y = 0,$$

which allows introducing the integral function of the current $U = -\psi_y, V = \psi_x$, where $U = U_1 + U_2, V = V_1 + V_2$ are the components of the total flows.

River runoff into the sea and water exchange through the straits are not taken into account. At the side basin boundaries the no-slip conditions and the condition $\Delta \mathbf{u}_k = 0$ are set. Initially, the water is at rest.

For numerical approximation, a time two-layer semi-implicit (economical explicit [4]) scheme was used implicit approximation of the Coriolis force and friction forces on the section and the bottom surface. Equations of motion and continuity were approximated on B -grid by the second accuracy order according to the scheme of central differences. It should be noted that in the previous experiments with a horizontal bottom, the nonlinear members in the continuity equations were approximated by the first accuracy order (directed differences) scheme and in the equations of motion – by the second accuracy order scheme of the (Lax – Wendroff) [4]. Approximation with central differences ensures compliance with the energy balance in the model.

In [1] it was shown that, due to the impact of nonlinear factors, even under the stationary wind effect, the solution of the problem eventually does not turn to a stationary, but to a quasi-periodic statistical-equilibrium state. At the same time, the inflow of energy from the wind to the sea is not constant and is regulated by the surface current field variability.

The energy inflow is implied to be the total work W_τ over the basin area, performed by the tangential wind stress, equal to the scalar product of the $\boldsymbol{\tau}$ and \mathbf{u}_1 vectors. Since the wind stress is stationary, the W_τ variability depends on the \mathbf{u}_1 variability.

Another important point to focus attention at is the bottom and horizontal friction consideration. The horizontal viscosity in this version of the model is parametrized by a bi-harmonic operator, in contrast to the previous experiments [1, 2],

where a harmonic operator was used. Bi-harmonic viscosity to a lesser extent prevents the appearance of synoptic and mesoscale vortices in the model [5].

The bottom friction in the experiments under consideration was parametrized by the formula $\mathbf{R}_b = (r_1 + r_2|\mathbf{u}_2|)\mathbf{u}_2$. The coefficient r_1 was set in order for bottom friction to act under weak currents. Friction at the interface of the layers was not taken into account ($\mathbf{R}_a = 0$) in the cases when $h_2 > 0$, in order to describe the formation of eddy structures (and the motion in general) in pure form in the lower layer. In those cases when $h_2 = 0$ and the upper layer was in contact with the bottom, $\mathbf{R}_a = (r_1 + r_2|\mathbf{u}_1|)\mathbf{u}_1$.

Numerical experiments. Below, the results of two numerical experiments R1 and R2 are given. In these experiments the motion in a two-layer sea with a real bottom relief $H(x, y)$ excited by a stationary wind stress $\boldsymbol{\tau}(x, y)$ having a constant cyclonic vorticity $\text{rot}_z(\boldsymbol{\tau}) = 2.53 \cdot 10^{-7} \text{ N/m}^3$ is considered. In the R1 experiment β -effect is taken into account, in R2 – it is neglected ($\beta = 0$). The tangential wind stress components τ^x, τ^y , as in [1, 2], were calculated according to the following formulas $\tau^x = \tau_S^x + y(\tau_N^x - \tau_S^x)/B$, $\tau^y = \tau_W^y + x(\tau_E^y - \tau_W^y)/L$, where $\tau_S^x = \tau_E^y = 0.5 \text{ cm}^2/\text{s}^2$, $\tau_N^x = \tau_W^y = -0.5 \text{ cm}^2/\text{s}^2$ – are set values of the $\boldsymbol{\tau}$ components on the northern, eastern, southern and western boundaries of the region ($0 < x < L$, $0 < y < B$), the Black Sea is inscribed.

In the initial time moment the h_0 upper layer thickness was equal to 175 m or to the sea depth H when $H < 175$ m. The bottom friction coefficients r_1, r_2 based on the previous calculations were selected to be equal to 0.001 and 0.002 cm/s respectively, the bi-harmonic viscosity coefficient $A_B = 4 \cdot 10^{16} \text{ cm}^4/\text{s}^4$. A rectangular grid with steps $\Delta x = \Delta y = 3 \text{ km}$ was applied, time step $\Delta t = 1.5 \text{ min}$.

The calculation duration in the both experiments was 20 years (one year consists of 12 months of 30 days each). During this period, both solutions reached a quasi-periodic statistical-equilibrium state. In this case, the area mean characteristics, namely the available potential energy DPE , the kinetic energy in the layers KE_1, KE_2 , the work of the tangential wind stress forces W_τ , of the bottom friction W_{RB} and the horizontal viscosity W_{AB}

$$\begin{aligned} DPE &= \langle \rho_1 g' h_1^2 / 2 \rangle - \langle \rho_1 g' h_0^2 / 2 \rangle, & KE_1 &= \langle \rho_1 h_1 (u_1^2 + v_1^2) / 2 \rangle, \\ KE_2 &= \langle \rho_2 h_2 (u_2^2 + v_2^2) / 2 \rangle, & W_\tau &= \langle \rho_1 (u_1 \tau^x + v_1 \tau^y) \rangle, \\ W_{RB} &= \sum_{k=1}^{k=2} \langle \rho_k (r_1 + r_2 \sqrt{u_k^2 + v_k^2}) (u_k^2 + v_k^2) \rangle, \\ W_{AB} &= \sum_{k=1}^{k=2} \langle \rho_k A_{LB} (u_k \nabla^2 (h_k \nabla^2 u_k) + v_k \nabla^2 (h_k \nabla^2 v_k)) \rangle \end{aligned}$$

changed only within certain limits with respect to some mean values (Fig. 1). Angular brackets mean averaging over the area.

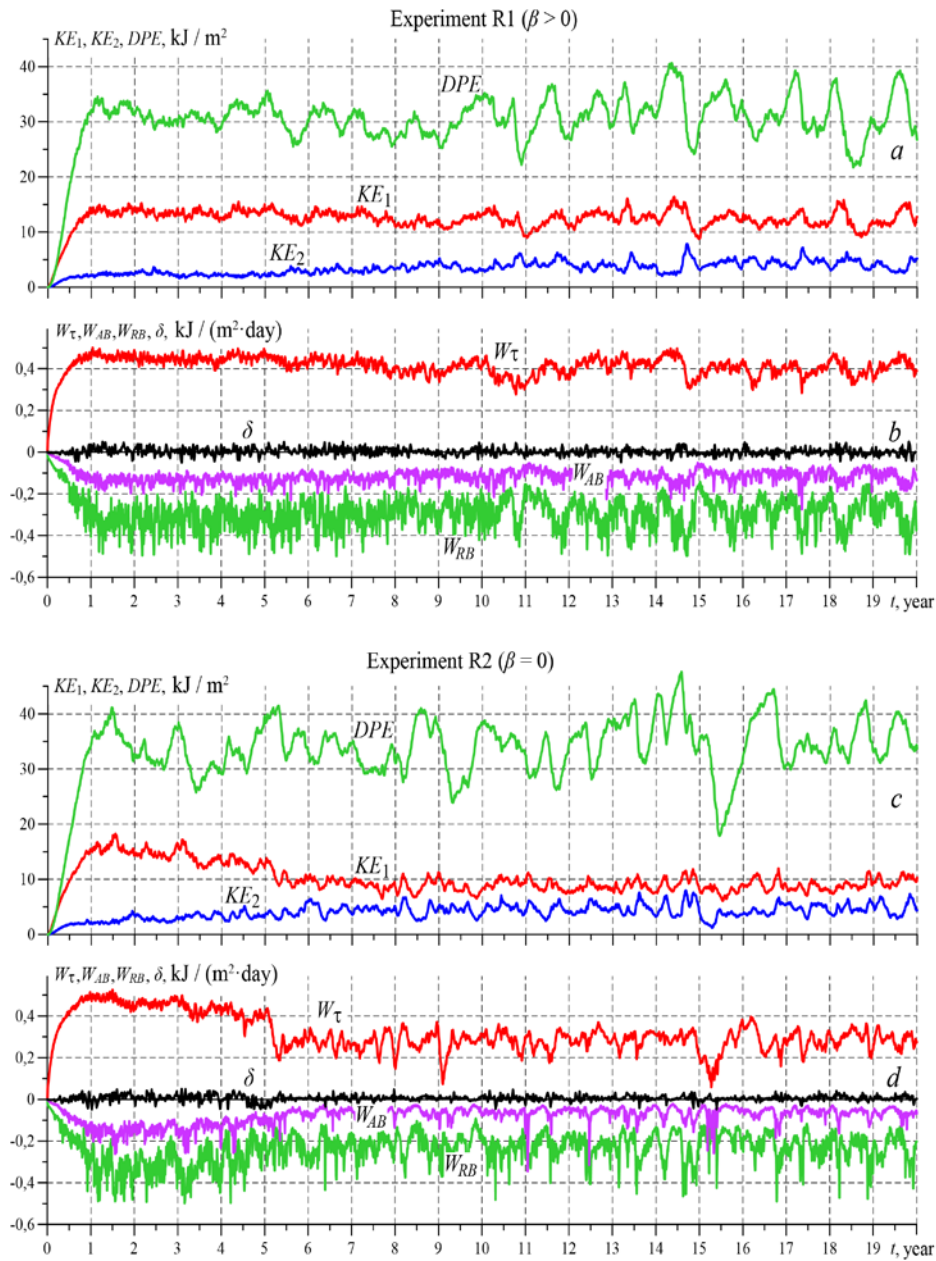


Fig. 1. Graphs of DPE , KE_1 , KE_2 in the R1 (a) and R2 (c) experiments; graphs of W_τ , W_{AB} , W_{RB} and δ in the R1 (b) и R2 (d) experiments

Energy and work of the forces satisfy the following equation of energy balance

$$\frac{\partial E}{\partial t} = W_\tau + W_{RB} + W_{AB} + \delta,$$

where $E = DPE + KE_1 + KE_2$; δ – a discrepancy due to the calculation accuracy of the energy balance components. As shown in Fig. 1, b, d, in the both experiments

R1 and R2, the energy balance is carried out with good accuracy during the entire computation period – δ is almost equal to zero.

The R1 experiment, $\beta > 0$. In this experiment, during the first year, DPE and KE_1 reach values within which their oscillations subsequently occur (Fig. 1, *a*). At that, the amplitude of these oscillations increases after the 10th year. The energy of KE_2 gradually increases during the first 10 years, then, after the solution is released to the statistically-equilibrium mode, also as DPE and KE_1 , oscillates relative to some mean value.

The work W_t (Fig. 1, *b*) varies in the similar way as KE_1 – is growing during the first year, then oscillates relative to the mean value characteristic of the statistically-equilibrium state. The W_{AB} and W_{RB} characteristics increase with the growth of KE_2 and decrease with its fall.

The attention to the presence of vibrations of two kinds on the graphs in Fig. 1, *a, b* should be drawn. Oscillations with a period of ~ 50 days, associated with hydrodynamic instability of flows in the upper layer, are clearly visible (especially in the graph of W_t). These high-frequency oscillations are superimposed on oscillations with periods from six months to two years. It can be assumed that such long-term oscillations are caused by the integral circulation variability.

Next, the analysis of the spatial fields obtained as a result of calculations is given. First, the averaged over the past 15 years \bar{h}_1 , $\bar{\mathbf{u}}_1$, $\bar{\mathbf{u}}_2$, $\bar{\mathbf{U}}_1$, $\bar{\mathbf{U}}_2$ and ψ fields are considered (Fig. 2).

In the mean fields of $\bar{\mathbf{u}}_1$ and $\bar{\mathbf{U}}_1$ (Fig. 2, *a, c*) a jet cyclonic stream located above the continental slope (the Black Sea Rim Current analog [6]) is observed. The velocity in this stream reaches 80 cm/s.

In the jet centerline, the \bar{h}_1 gradients are maximum, to the left of the centerline to the basin center \bar{h}_1 decreases, to the right towards the coast – increases. To the west of the Crimea and in the south-eastern part of the sea there are local areas with high \bar{h}_1 values. These are the Sevastopol and Batumi anticyclones [7].

The average currents in the lower layer are also cyclonic, but unlike the currents in the upper layer, they are attached to the bottom relief features and are directed predominantly along the H isobaths (Fig. 2, 3). The highest velocities of currents (up to 17 cm/s) are observed on the continental slope in places of sharp continental slope and near the intersection of the interface with the bottom, where the thickness of the lower layer is rather small. Despite the fact that the current velocities in the lower layer are much smaller than in the upper layer, the flows in the lower layer, on the contrary, exceed the ones in the upper layer. The reason for this is a large difference in the thicknesses of the layers. This leads to the fact that the integral function of current ψ (Fig. 2, *f*) reflects the flows in the lower layer to a greater extent, in the deep part of the sea especially, where the lower layer thickness is large.

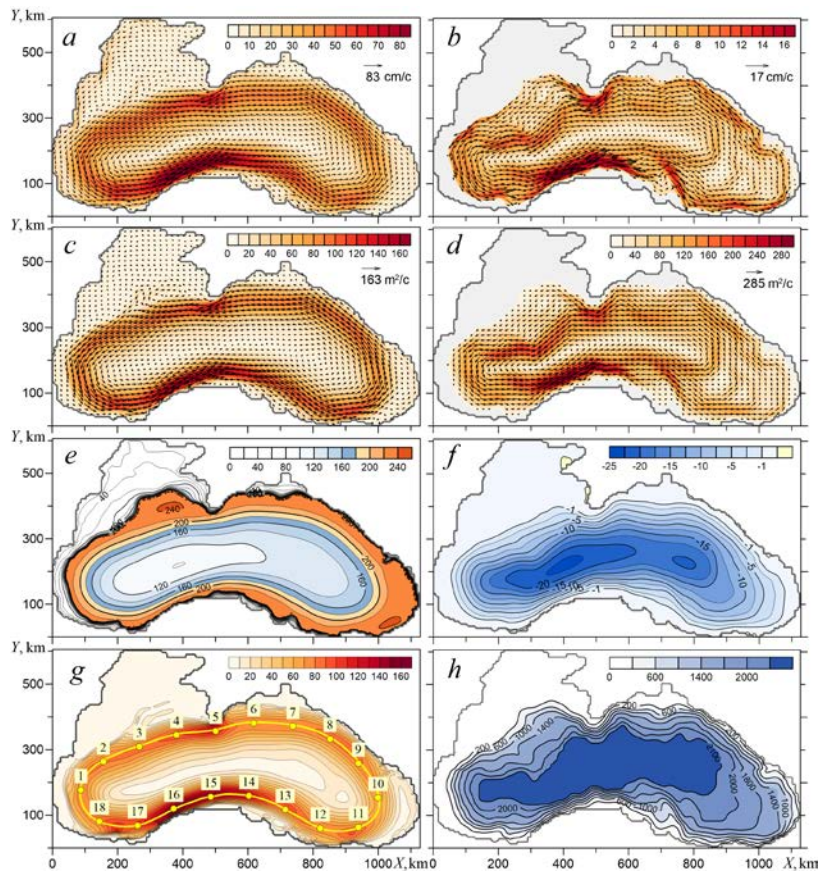


Fig. 2. Averaged over 15 years $\bar{\mathbf{u}}_1$ (a), $\bar{\mathbf{u}}_2$ (b), $\bar{\mathbf{U}}_1$ (c), $\bar{\mathbf{U}}_2$ (d), \bar{h}_1 (e) and $\bar{\psi}$ (f) fields in the R1 experiment; module of the mean flows in the upper layer $|\bar{\mathbf{U}}_1|$ and isoline $\bar{h}_1 = 200$ m with control points (g); bottom relief $H(x, y)$ (h). On the maps $\bar{\mathbf{u}}_1$, $\bar{\mathbf{u}}_2$, $\bar{\mathbf{U}}_1$ and $\bar{\mathbf{U}}_2$ the maximum values are indicated under the arrows, the color scales correspond to absolute values

Next the instantaneous fields obtained in the R1 experiment are considered. In Fig. 3, *a – f* the h_1 , \mathbf{u}_1 , \mathbf{u}_2 , \mathbf{U}_1 , \mathbf{U}_2 and ψ fields are given for a single time moment. They are quite typical for a statistically-equilibrium state. In the upper layer in the \mathbf{u}_1 and \mathbf{U}_1 fields, a jet meandering current is clearly visible. It is located above the continental slope along the entire perimeter of the basin. From the analysis of the results it follows that the meanders propagate in the direction of the jet in the form of waves with a phase velocity that is less than the current velocity. The jet width is 30 – 50 km, the velocity in the centerline is 80 – 120 cm/s. Anticyclonic and cyclonic eddies are observed to the right and left of the stream, respectively. Their formation is a consequence of the meandering of the Rim current, as well as the flow around the coastline features. In addition, anticyclonic rings are periodically formed to the left of the jet as a result of the detachment of large meanders. Fig. 3, *a* shows the formation of such a ring in the northeastern part of the basin.

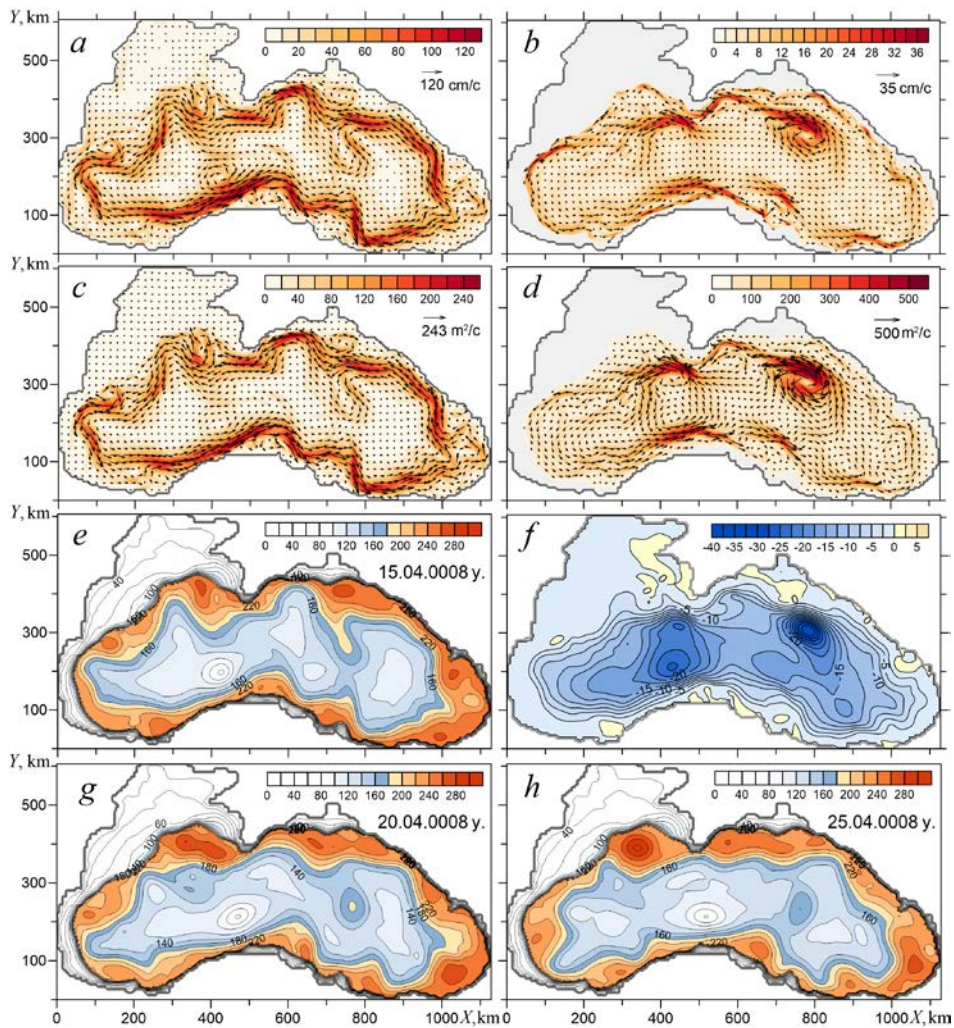


Fig. 3. Instantaneous fields of \mathbf{u}_1 (a), \mathbf{u}_2 (b), \mathbf{U}_1 (c), \mathbf{U}_2 (d), h_1 (e) and ψ (f) in the R1 experiment for the time moment 15.04.000; the h_1 field for the time moment 20.04.0008 (g); the h_1 field for the time moment 25.04.0008 (h). On the maps $\bar{\mathbf{u}}_1$, $\bar{\mathbf{u}}_2$, $\bar{\mathbf{U}}_1$ and $\bar{\mathbf{U}}_2$ the maximum values are indicated under the arrows, the color scales correspond to absolute values

As already noted, the h_1 field is closely related to the field of currents and flows in the upper layer. In anticyclones, the interface of the layers is lowered (the upper layer thickness increases), in cyclones it rises (h_1 decreases), the h_1 gradients become aggravated in the area of the jet flows. Due to this, all the features of the circulation of the upper layer (jet flows, meanders and eddies) are clearly visible in the h_1 field (Fig. 3, d). By successive h_1 distributions with an interval of 5 days (Fig. 3, e, g, h), the upper layer dynamics, the movement of meanders along the main stream and the formation of a ring can be traced.

In the lower layer, under a predominantly cyclonic orientation of currents and flows, the circulation pattern is different than in the upper layer. There is no circular jet stream. The observed flows are irregular in nature, they look like separate jets

stretched along the isobaths and also moving along the continental slope. This occurs as a result of the imposition of intense waves and/or eddies on the middle stream.

Velocities of the currents in the lower layer do not exceed 5 cm/s in its greater part, they are $\sim 10\text{--}15$ cm/s in the jets, and near the intersection of the interface with the bottom, where the lower layer thickness h_2 is small, they can reach 35 cm/c. The appearance of unreal high velocities in thin layers is apparently due to the quite incorrect consideration of bottom friction. Such flows should not be given much importance, since in the flows such features do not appear in thin layers (Fig. 3, *d*).

Owing to the large difference in the thicknesses of the layers, the flows in the lower layer are larger in magnitude than in the upper layer (Fig. 3, *c, d*). This leads to the fact that the integral current function ψ (Fig. 3, *e*) reflects the nature of the circulation of the lower layer to a greater extent, especially in the deep-water part of the sea.

To identify the wave processes in the continental slope area, timing diagrams $h_1'(t) = h_1(t) - \overline{h_1}$ and $\psi'(t) = \psi(t) - \overline{\psi}$ were constructed along the isoline $\overline{h_1} = 200$ m, practically coinciding with the averaged flow centerline in the upper layer (Fig. 2, *g*) and located in the continental slope area approximately above the 1,600 m isobath. Here the control points with an interval of 120 km are selected. On the timing diagrams (Fig. 4), they correspond to vertical dotted lines; the number of points is indicated on the upper boundary. In the both diagrams, it is clearly seen that perturbations in the form of waves propagate along the continental slope in a counterclockwise direction. The propagation velocities of these waves differ for different sections of the trajectory. So, the waves move faster along the southern coast than along the northern one. Most likely, this is due to the different steepness of the continental slope. In the area 15–13–10 (Fig. 4), except the marked waves, slower perturbations are observed. They are associated with the formation of anticyclonic eddies in the Anatolian coast region.

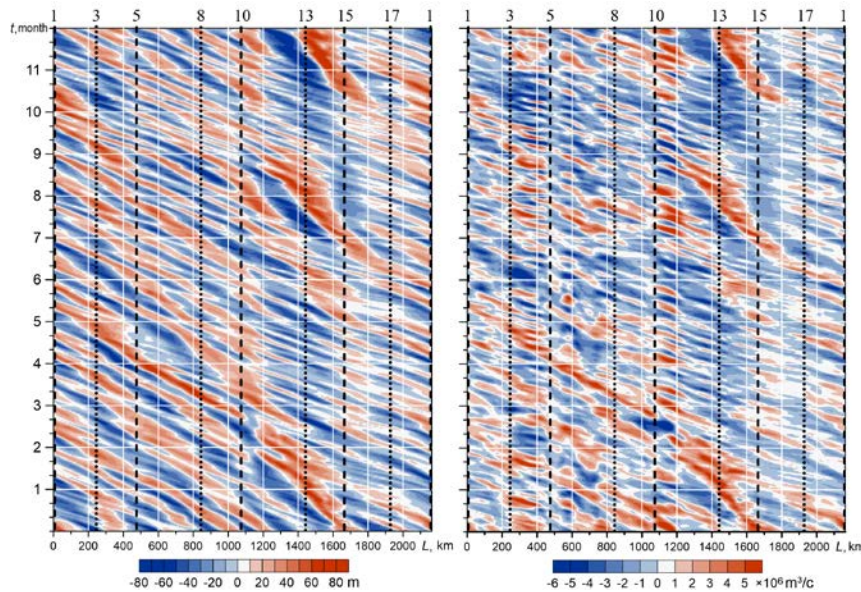


Fig. 4. Timing diagrams of $h_1'(t)$, m, (left) and $\psi'(t)$, $\times 10^6$ m³/s, (right) along the isoline $\overline{h_1} = 200$ m b during the 10th year

There is a large external similarity between the two diagrams, which indicates a close relationship of wave processes in different layers. At that, the diagram $h_1'(t)$ reflects the wave processes occurring in the upper layer, and the diagram $\psi'(t)$ demonstrates the dynamics of the integral circulation, the greater contribution to which the lower layer makes. Note that in the diagram $\psi'(t)$ against the background of longer waves, the pulsations associated with topographic effects are visible.

According to the slope of the phase lines (Fig. 4), the propagation velocity of the waves, which is ~ 19 cm/s in the area 1–15–10 and ~ 16 cm/s in the area 10–5–1 can be calculated. The obtained phase velocity values are comparable with the mean values of the velocity of currents in the lower layer, but they are much smaller than the average velocities of the currents in the upper layer in the Black Sea Rim Current area.

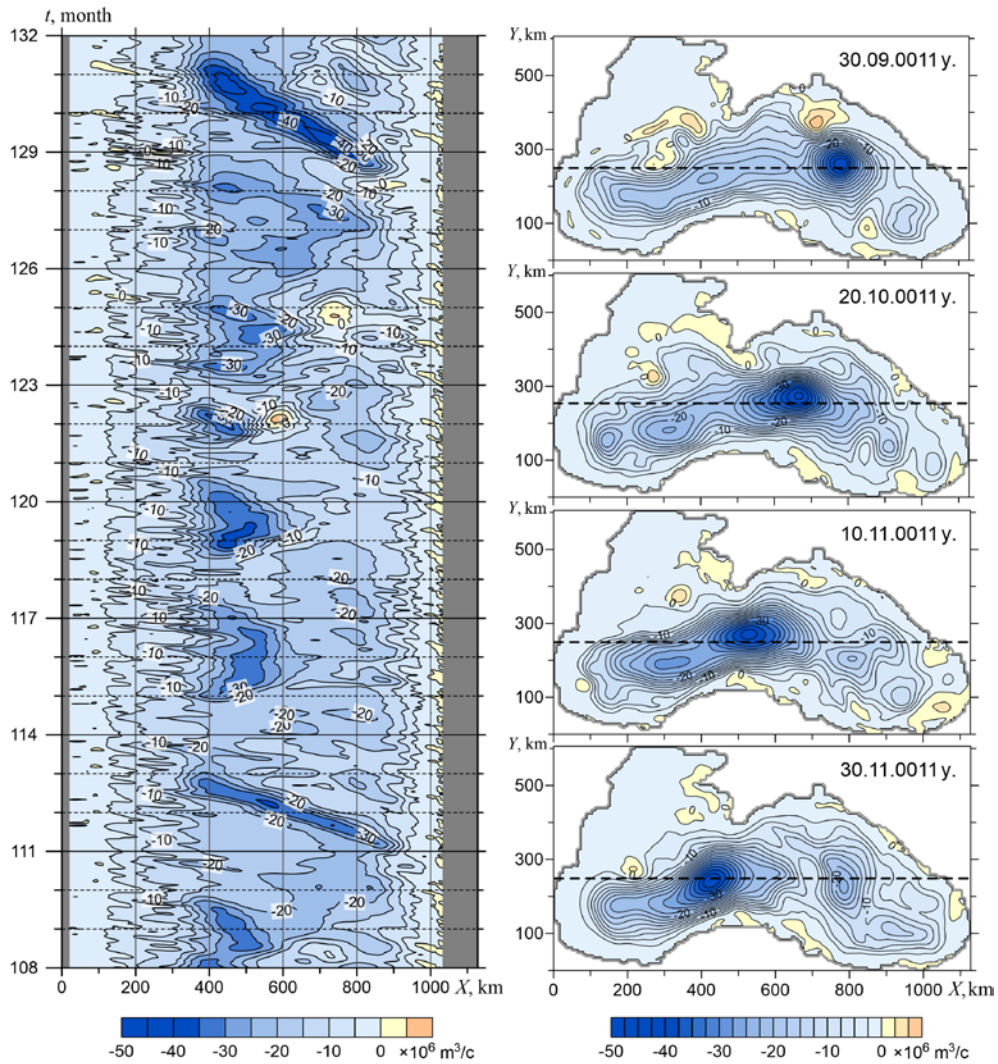


Fig. 5. Timing diagrams $\psi(t)$, $\times 10^6$ m³/s, for a $Y = 250$ km section from 10th to 11th year in the R1 experiment (left) and successive 20 day interval fields ψ , $\times 10^6$ m³/s, (right). The section is shown by a dashed line

To determine the frequency characteristics of waves, the time series $h_1(t)$ and $\psi(t)$ at the control points were studied by the spectral analysis method [8]. On the constructed spectral density graphs $S_h(\nu)$, $S_\psi(\nu)$, significant peaks at frequencies $\nu_1 \approx 0.021$ and $\nu_2 \approx 0.036$ 1/day are allocated for all the points considered, which indicates the discrete nature of the observed waves. These frequencies correspond to the periods of oscillations $T_1 \approx 48$ and $T_2 \approx 27$ days. The results obtained agree with the analytical estimates given in [9, 10].

Except the waves spreading over the continental slope, in the central deep part of the sea, Rossby waves were identified in the $\psi(t)$ field, moving westward. Fig. 5 is a timing diagram $\psi(t)$ constructed for a $Y = 250$ km section. It can be seen that for two years (10–11th year) such a wave was clearly manifested twice, in April – May of the 10th year and in October – November of the 11th year. The phase velocity of the wave, calculated from the slope of the phase lines, is ~ 7.5 cm/s and corresponds to the phase velocity of the first normal mode of the barotropic Rossby wave for a closed basin with a horizontal bottom [11 – 13]. The propagation of this wave is shown in successive (with an interval of 20 days) distributions of the integral current function from September 30 to November 30 of the 11th year.

The R2 experiment, $\beta = 0$. In the β -effect absence, the circulation formation process during the first 5 years is similar to the process in the R1 experiment. In both layers in the continental slope region, currents are formed and develop, propagating along the entire perimeter of the Black Sea. These waves were superimposed by wave perturbations related to the bottom relief flowing around (Rossby topographic waves [9, 14, 15]). The graphs of available potential energy, kinetic energy, work of tangential wind forces, bottom friction and horizontal viscosity in the R2 experiment (Fig. 1, *c, d*) in the first 5 years differ little from similar graphs in the R1 experiment (Fig. 1, *a, b*). Also, during this period, the spatial distributions of the flows, the upper layer thickness and the integral function of the current are qualitatively and even quantitatively close to the distributions obtained taking into account the β -effect.

Since the 6th year, the circulation pattern in the R2 experiment changes and takes the form shown in Fig. 6. Unlike the R1 experiment, the main cyclonic gyre does not extend to the entire basin, but shrinks to its central part. This can be seen both in the instantaneous (Fig. 6, *a, c, e, g*) and in the averaged fields (Fig. 6, *b, d, f, h*).

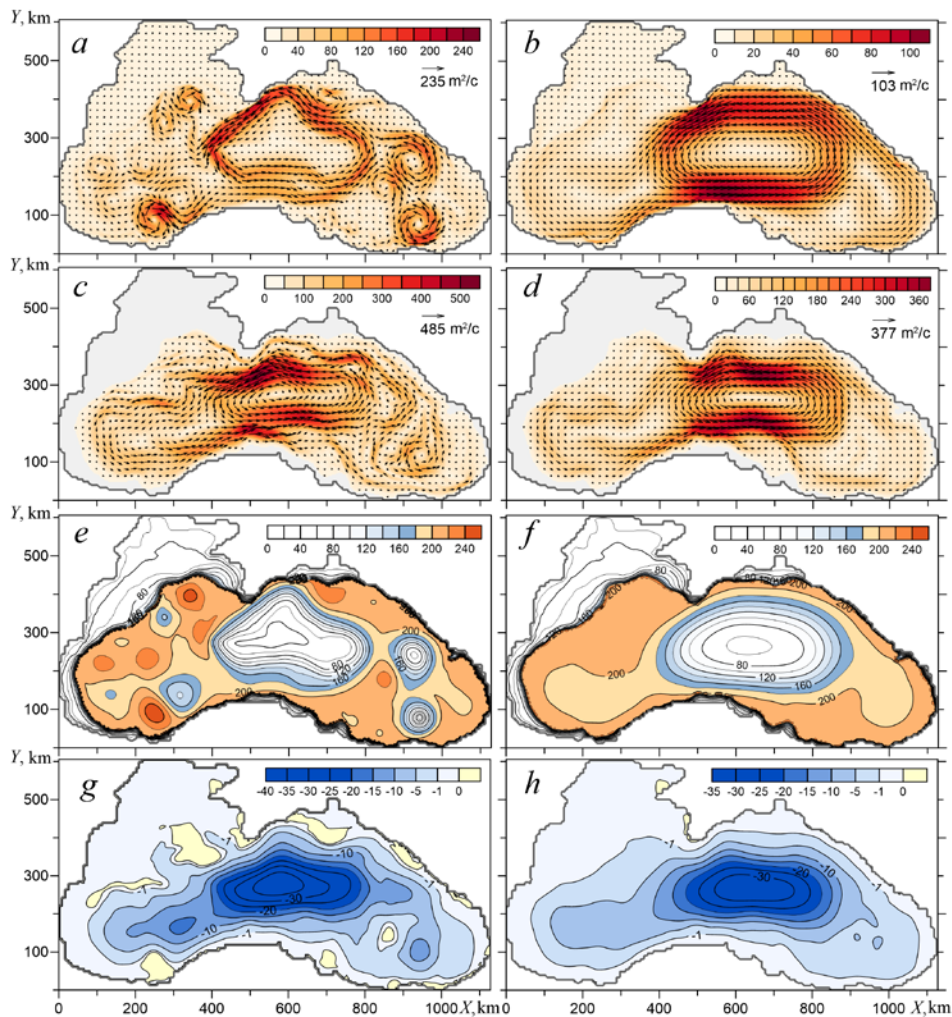


Fig. 6. Instantaneous (for 30.12.0020) and averaged over 15 years fields in the R2 experiment: U_1 (a); \bar{U}_1 (b); U_2 (c); \bar{U}_2 (d); h_1 (e); \bar{h}_1 (f); ψ (g); $\bar{\psi}$ (h). On the maps U_1 , \bar{U}_1 , U_2 , \bar{U}_2 the maximum values are indicated under the arrows, the color scales correspond to absolute values

Conclusion. Based on the comparison of the results of the R1 and R2 experiments the following conclusions can be drawn.

Long-term cyclonic wind impact, taking into account the real bottom topography and the β -effect, leads to the formation of a meandering jet cyclonic flow in the basin (the Black Sea Rim Current analog) with centerline located in the continental slope area. Long-wave oscillations (Rossby topographic waves) are superimposed on this current, both in the upper and lower layers. According to their parameters and the nature of manifestation, these oscillations correspond to waves trapped by the continental slope and propagating in the cyclonic direction.

The change of the Coriolis parameter with latitude (β -effect) in the Black Sea, in addition to its effect on the topographic Rossby waves, also manifests itself in the formation in the central deep part of the barotropic Rossby waves for a closed basin

extending from east to west. The absence of these waves leads to the fact that the circular current does not extend to the entire sea, but is localized in its central part.

Acknowledgements. The work was carried out within the framework of the State Order No. 0827-2014-0011 *Research of the Regularities of Changes in the Condition of the Marine Environment on the Basis of Operational Observations and Data of the System of Diagnosis, Prognosis and Reanalysis of the Condition of Marine Areas (Operational Oceanography)*.

REFERENCES

1. Pavlushin, A.A., Shapiro, N.B., Mikhailova, E.N. and Korotaev, G.K., 2015. Two-Layer Eddy-Resolving Model of Wind Currents in the Black Sea. *Physical Oceanography*, [e-journal] (5), pp. 3-12. doi:10.22449/1573-160X-2015-5-3-21
2. Pavlushin, A.A., Shapiro, N.B. and Mikhailova, E.N., 2016. Display of the β -effect in the Black Sea Two-Layer Model. *Physical Oceanography*, [e-journal] (5), pp. 3-23. doi:10.22449/1573-160X-2016-5-3-23
3. Holland, W.R. and Lin, L.B., 1975. On the Generation of Mesoscale Eddies and their Contribution to the Oceanic General Circulation. I. A Preliminary Numerical Experiment. *J. Phys. Oceanogr.*, [e-journal] 5(4), pp. 642-657. doi:10.1175/1520-0485(1975)005<0642:OTGOME>2.0.CO;2
4. Mesinger, F. and Arakawa, A., 1976. Numerical Methods Used in Atmospheric Models. *GARP Publ. Ser.*, No. 17. 64 p. Available at: http://twister.ou.edu/CFD2003/Mesinger_ArakawaGARP.pdf [Accessed: 12 April 2017].
5. Kamenkovich, V.M., Koshlyakov, M.N. and Monin, A.S., 1987. *Sinopticheskie Vikhri v Okeane* [Synoptical Eddies in the Ocean]. Leningrad: Gidrometeoizdat, 510 p. (in Russian).
6. Blatov, A.S., Bulgakov, N.P., Ivanov, V.F., Kosarev, A.N. and Tuzhilkin, V.S., 1984. *Izmenchivost' Gidrofizicheskikh Poley Chernogo Morya* [Variability of Hydrophysical Fields of the Black Sea]. Leningrad: Gidrometeoizdat, 239 p. (in Russian).
7. Ivanov, V.A. and Belokopytov, V.N., 2011. *Okeanografiya Chernogo Morya* [Oceanography of the Black Sea]. Sevastopol: MHI NANU, 212 p. (in Russian).
8. Nussbaumer, H.J., 1982. Fast Fourier Transform and Convolution Algorithms. [e-book] New York: Springer-Verlag, 286 p. Available at: URL: https://proofwiki.org/wiki/Book:H.J._Nussbaumer/Fast_Fourier_Transform_and_Convolution_Algorithms/Second_Edition [Accessed: 15 April 2017].
9. Efimov, V.V., Kulikov, E.A., Rabinovich, A.B. and Fayn, I. V., 1985. *Volny v Pogranichnykh Oblastyakh Okeana* [Waves in the Boundary Regions of the Ocean]. Leningrad: Gidrometeoizdat, 280 p. (in Russian).
10. Ivanov, V.A. and Yankovsky, A.E., 1992. *Dlinnovolnovye Dvizheniya v Chernom More* [Long-Wave Motion in the Black Sea]. Kiev: Naukova Dumka, 110 p. (in Russian).
11. Rachev, N.H. and Stanev, E.V., 1997. Eddy Processes in Semienclosed Seas: A Case Study for the Black Sea. *J. Phys. Oceanogr.*, [e-journal] 27(8), pp. 1581-1601. doi:10.1175/1520-0485(1997)027<1581:EPISSA>2.0.CO;2
12. Stanev, E.V. and Rachev, N.H., 1999. Numerical Study on the Planetary Rossby Modes in the Black Sea. *J. Marine Syst.*, [e-journal] 21(1-4), pp. 283-306. doi:10.1016/S0924-7963(99)00019-6
13. Kamenkovich, V.M. and Monin, A.S., 1978. *Fizika Okeana. T. 2 – Gidrodinamika Okeana* [Ocean Physics. Vol. 2 – Ocean Hydrodynamics]. Moscow: Nauka, 435 p. (in Russian).
14. Longuet-Higgins, M.S., 1965. Planetary Waves on a Rotating Sphere. II. *Proc. R. Soc. Lond. A. Math. Phys. Sci.*, [e-journal] 284(1396), pp. 40-68. doi:10.1098/rspa.1965.0051
15. Monin, A.S. and Zhikharev, G.M., 1990. Ocean Eddies. *Soviet. Physics Uspekhi*, 33(5), pp. 313-339. doi:10.1070/PU1990v033n05ABEH002569